

Large thermoelectric performance of heavily Nb-doped SrTiO₃ epitaxial film at high temperature

Shingo Ohta and Takashi Nomura

Nagoya University, Graduate School of Engineering, Furo-cho, Chikusa, Nagoya 464-8603, Japan

Hiromichi Ohta

Nagoya University, Graduate School of Engineering, Furo-cho, Chikusa, Nagoya 464-8603, Japan, CREST, JST, 4-1-8 Motomachi, Kawaguchi 332-0012, Japan, and ERATO-SORST, JST, in Frontier Collaborative Research Center, Mail Box S2-13, Tokyo Institute of Technology, 4259 Nagatsuta, Midori, Yokohama 226-8503, Japan

Masahiro Hirano

ERATO-SORST, JST, in Frontier Collaborative Research Center, Mail Box S2-13, Tokyo Institute of Technology, 4259 Nagatsuta, Midori, Yokohama 224-8503, Japan

Hideo Hosono

ERATO-SORST, JST, in Frontier Collaborative Research Center, Mail Box S2-13, Tokyo Institute of Technology, 4259 Nagatsuta, Midori, Yokohama 226-8503, Japan and Frontier Collaborative Research Center, Mail Box S2-13, Tokyo Institute of Technology, 4259 Nagatsuta, Midori, Yokohama 226-8503, Japan

Kunihito Koumoto^{a)}

Nagoya University, Graduate School of Engineering, Furo-cho, Chikusa, Nagoya 464-8603, Japan and CREST, JST, 4-1-8 Motomachi, Kawaguchi 332-0012, Japan

(Received 14 February 2005; accepted 11 July 2005; published online 26 August 2005)

Carrier concentration dependence of the thermoelectric figure of merit, ZT of SrTiO₃ at high-temperature (1000 K) is clarified using heavily Nb-doped SrTiO₃ epitaxial films, which were grown on insulating (100)-oriented LaAlO₃ single-crystalline substrates by a pulsed-laser deposition method. Carrier concentration, Hall mobility, Seebeck coefficient, and thermal conductivity of Nb-doped SrTiO₃ epitaxial films were experimentally evaluated at 1000 K with an aid of theoretical analysis. ZT of Nb-doped SrTiO₃ increases with Nb concentration and it reaches ~ 0.37 (20% Nb doped), which is the largest value among n -type oxide semiconductors ever reported. © 2005 American Institute of Physics. [DOI: 10.1063/1.2035889]

Recently, cobalt-based p -type oxide semiconductors including Na_xCoO₂,¹ Ca₃Co₄O₉,² and their derivatives,^{3,4} which exhibit rather high thermoelectric figure of merit ($ZT = S^2\sigma/\kappa$, where, T , S , σ , and κ are absolute temperature, Seebeck coefficient, electrical conductivity, and thermal conductivity, respectively), have attracted growing attention for the realization of thermoelectric power generation operating at high temperatures⁵ because they have potential advantages over conventional high-temperature thermoelectric semiconductors including SiGe-based alloy ($ZT \sim 1$)⁶ and β -FeSi₂ ($ZT \sim 0.3$)⁷ in terms of chemical and thermal resistance at high-temperatures (~ 1000 K). On the other hand, n -type oxide semiconductors, which are inevitably required as a partner of the p -type oxide semiconductors to develop thermoelectric power generation modules, have exhibited rather low ZT values of ~ 0.3 for Al-doped ZnO at 1273 K (see Ref. 8) and ~ 0.31 for In₂O₃(ZnO) m (m =integer) at 1073 K.^{9,10} Hence, it is necessary to improve ZT of these compounds or to explore novel oxide materials with large ZT values.

We focused on heavily carrier-doped SrTiO₃ as a promising candidate of n -type oxide semiconductor because it exhibits rather large $|S|$ due to the large carrier effective mass ($m^* = 6 - 10 m_0$).¹¹ Further, bulk single crystals of heavily La-

doped SrTiO₃ have recently been found to have large power factor ($PF = S^2\sigma$) of $3.6 \times 10^{-3} \text{ W m}^{-1} \text{ K}^{-2}$ at room temperature,¹² which is comparable to that of practical Peltier material Bi₂Te₃.¹³

Very recently, we have examined carrier transport properties of Nb- and La-doped SrTiO₃ single crystals (carrier concentration, n , up to $\sim 10^{20} \text{ cm}^{-3}$) at high temperatures (~ 1000 K) to clarify their thermoelectric response.¹⁴ Although the experimental data suggested that fairly high ZT is expected in heavily Nb-doped SrTiO₃, the optimization of ZT could not be achieved because the solubility of the Nb dopants in the SrTiO₃ lattice is substantially small, making it impossible to get an optimal dopant concentration. In order to overcome this problem, we fabricated SrTiO₃ epitaxial films having $\sim 10^{22} \text{ cm}^{-3}$ Nb as the dopant on the (100)-oriented LaAlO₃ substrate by a pulsed-laser deposition (PLD). Here we report high-temperature (1000 K) thermoelectric performance of the heavily Nb-doped SrTiO₃. The 20% ($4 \times 10^{21} \text{ cm}^{-3}$) Nb-doped SrTiO₃ epitaxial film exhibited $ZT \sim 0.37$ at 1000 K, which is the largest value among n -type oxide semiconductors ever reported.

Epitaxial films of Nb-doped SrTiO₃ were grown on (100)-oriented LaAlO₃ single-crystalline substrates at 700 °C by PLD (4 ω -Nd:yttrium-aluminum-garnet (YAG) laser, $\lambda = 266 \text{ nm}$, $\sim 1 \text{ J cm}^{-2} \text{ pulse}^{-1}$, $\sim 20 \text{ ns}$, 10 Hz) using SrTiO₃ targets containing up to 40% Nb as dopant. High-resolution x-ray diffraction (XRD) (ATX-G, Rigaku Co.) measurements revealed that the Nb-doped SrTiO₃ were grown heteroepi-

^{a)} Author to whom correspondence should be addressed; electronic mail: g44233a@nuccl.nagoya-u.ac.jp

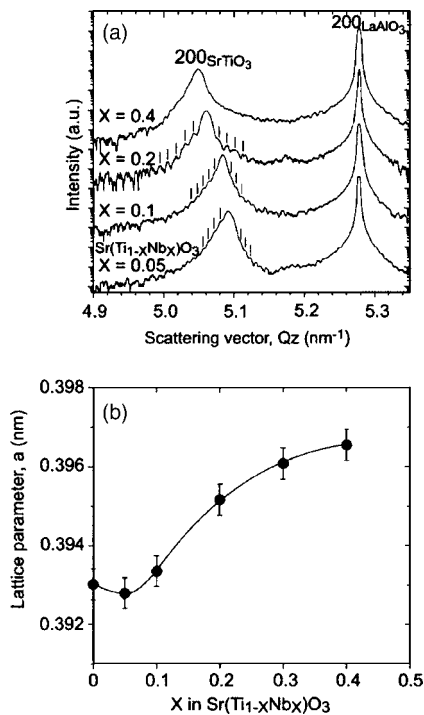


FIG. 1. (a) Out-of-plane XRD patterns of Nb-doped SrTiO₃ epitaxial films grown on the (100)-oriented LaAlO₃ substrate at 700 °C. Thickness fringes are clearly seen around 200 SrTiO₃ as indicated by solid lines. (b) Change in the lattice parameter of the SrTiO₃ films as a function of the Nb concentration. The solid line is a guide for eye.

taxially on the substrate. Figure 1(a) shows out-of-plane XRD patterns of the Nb-doped film grown on the (100)-oriented LaAlO₃ substrate at 700 °C by PLD. Only an intense Bragg diffraction peak of 200 SrTiO₃ is observed together with 200 LaAlO₃. Pendellosung fringes are clearly observed around the 200 SrTiO₃ peak indicating high-crystalline qualities of the films. Film thicknesses were calculated from the Pendellosung fringes to be 118 nm (10% Nb-doped), 82 nm (20%), 130 nm (30%), and 96 nm (40%). The lattice parameter of the Nb-doped SrTiO₃ films increases proportionally to Nb concentration [Fig. 1(b)] indicating that Nb⁵⁺ (64.0 pm) is substituted at Ti⁴⁺ (60.5 pm) site.¹⁵ This site selectivity of Nb is also supported by the fact that Nb⁵⁺ ions act as a donor.

The electrical conductivity (σ), carrier concentration (n), Hall mobility (μ), and Seebeck coefficient (S) for the Nb-doped SrTiO₃ epitaxial films were measured from RT to 1000 K. The n value was independent of temperature, while the μ value decreased proportionally to $T^{-1.5}$ above the Debye temperature of SrTiO₃ ($\theta_D = 693$ K),¹⁶ indicating that the acoustic phonon plays a dominant role in the carrier scattering mechanism. On the other hand, the $|S|$ values gradually increased with temperature due to the monotonic decrease in chemical potential. As a result, the power factor ($PF = S^2\sigma$) value increased gradually with temperature, which is basically the same as that of Nb-doped SrTiO₃ bulk single crystal.¹⁴ In order to clarify the optimal Nb concentration, we focused on high-temperature (1000 K) thermoelectric properties of the Nb-doped SrTiO₃ epitaxial films.

Figure 2(a) shows n and μ of the Nb-doped SrTiO₃ epitaxial films, measured by dc four probe method using van der Pauw configuration at 1000 K under a high-vacuum ($\sim 10^{-3}$ Pa) condition. The n value increases proportional to the Nb concentration of the film and it agrees well with that

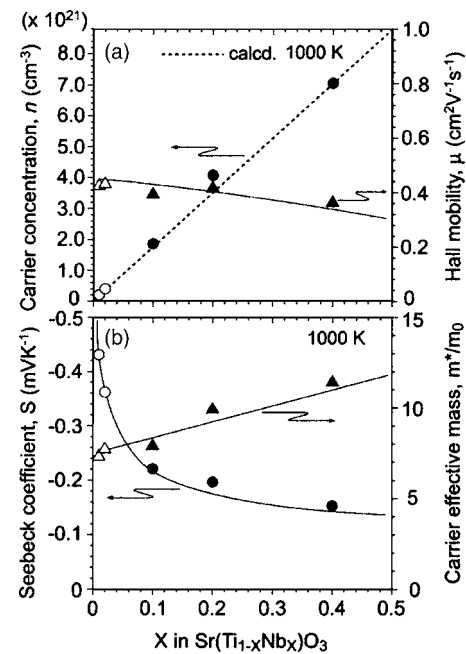


FIG. 2. Thermoelectric properties of Nb-doped SrTiO₃ epitaxial films at 1000 K (solid circles and triangles). Those for single crystals are shown by open circle and triangle for comparison. (a) Carrier concentration (n) and Hall mobility (μ) as a function of the Nb concentration. The dotted line for n is an estimated value from the Nb content. The solid line for μ is a calculated value from m^* . (b) Seebeck coefficient (S) and carrier effective mass (m^*) as a function of the Nb concentration. Both solid lines for S and m^* are guide for eye.

estimated from the Nb concentration, indicating that substituted Nb⁵⁺ at Ti⁴⁺ site fully generates carrier electrons. In other words, n of SrTiO₃ films is controlled up to $\sim 10^{22}$ cm⁻³ by the Nb doping. On the other hand, μ for the Nb-doped SrTiO₃ films decreased gradually with the Nb concentration. It is likely due to the fact that the carrier effective mass (m^*) for the Nb-doped SrTiO₃ films gradually increased with the Nb concentration. Thus, the mean free path of the carrier electron in the Nb-doped SrTiO₃ was almost independent of the Nb concentration, which indicates that the contribution of the ionized impurity scattering to the carrier mobility is rather small.

Figure 2(b) shows n dependence of $|S|$ in the Nb-doped SrTiO₃ epitaxial films, measured by the conventional steady state method under high-vacuum ($\sim 10^{-3}$ Pa). Contribution of the LaAlO₃ substrate to the Seebeck voltage, S , is negligible because the substrate is electrically insulating, which is further supported by the agreement of the S values at the low carrier concentration between slightly Nb-doped SrTiO₃ epitaxial film and bulk single crystalline SrTiO₃. $|S|$ decreases gradually with n having negative values in all the concentration, indicating that the Nb-doped SrTiO₃ epitaxial films are an n -type semiconductor. It is noted that a rather large $|S|$ (0.16 mV K⁻¹) is observed for the 40%-Nb-doped SrTiO₃ film in spite of an extremely high carrier concentration ($\sim 7 \times 10^{21}$ cm⁻³).

In order to clarify the reason for the large $|S|$ value, we calculated the carrier effective mass, m^* , of the Nb-doped SrTiO₃ films at 1000 K because S correlates strongly with m^* . The m^* is estimated using the following equations¹⁷ and the observed S value:

$$m^* = \frac{h^2}{2k_B T} \left[\frac{n}{4\pi F_{1/2}(\xi)} \right]^{2/3}, \quad (1)$$

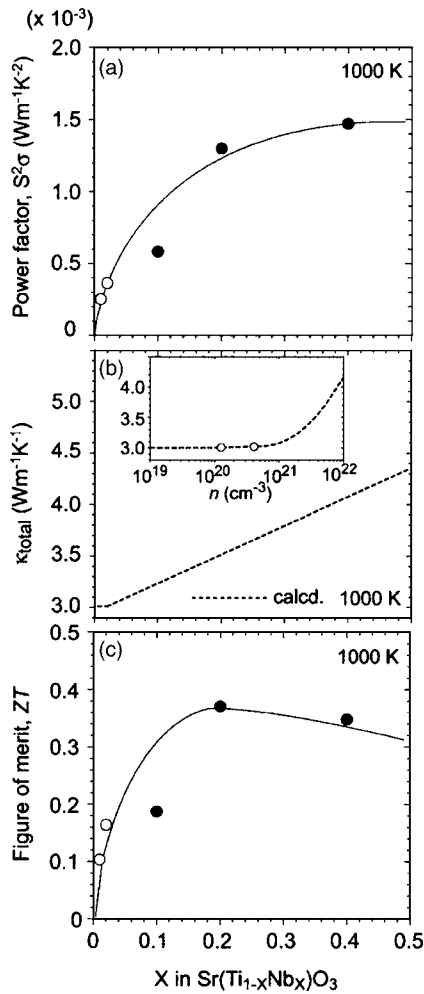


FIG. 3. Nb concentration dependence of thermoelectric parameters for Nb-doped SrTiO_3 epitaxial films at 1000 K. Open circles are for the single crystals and solid circles are for the films. The solid line is guide for eye. (a) Power factor (PF). (b) Calculated thermal conductivity (κ_{total}). Inset shows the carrier concentration (logarithm scale) dependence of κ_{total} . (c) Figure of merit (ZT).

$$F_r(\xi) = \int_0^\infty \frac{x^r}{1 + e^{x-\xi}} dx, \quad (2)$$

$$S = -\frac{k_B}{e} \left[\frac{(r+2)F_{r+1}(\xi)}{(r+1)F_r(\xi)} - \xi \right], \quad (3)$$

where, h , k_B , T , F_r , ξ , and r are, the Planck constant, the Boltzmann constant, absolute temperature ($T=1000$ K), Fermi integral, chemical potential, and the carrier scattering parameter of relaxation time, respectively. Here we neglect r since r becomes zero in the acoustic phonon scattering mechanism. The m^*/m_0 value, where m_0 is free electron mass, increases monotonically from ~ 7 ($x=0$) to ~ 11 ($x=0.4$) with n as shown in Fig. 2(b). The μ values calculated using the m^* values agree well with the observed m^* values as shown in Fig. 2(a), showing the validity of our analysis. From these results, we conclude that the large $|S|$ values in high carrier concentration films result from the gradual increase in m^*/m_0 with n . The enhancement of m^* is partly due to an increase in the lattice parameter or an increase in the distance between two neighboring Ti ions, which leads to a decrease in the overlapping between Ti $3d-t_{2g}$ orbitals.

PF values ($S^2\sigma$) of Nb-doped SrTiO_3 at 1000 K are plotted in Fig. 3(a). PF increases gradually with carrier concentration and it becomes saturated with further increase in n , exhibiting the maximum of $\sim 1.5 \times 10^{-3} \text{ Wm}^{-1}\text{K}^{-2}$ for the 40%-Nb-doped SrTiO_3 film, which is approximately half of practically used SiGe alloys.⁶ Then, we estimate thermal conductivity (κ_{total}) according to the Wiedemann-Franz law expressed by Eqs. (4) and (5):

$$\kappa_{\text{total}} = \kappa_{\text{lattice}} + \kappa_{\text{electron}}, \quad (4)$$

$$\kappa_{\text{electron}} = L\sigma T, \quad (5)$$

where, κ_{lattice} , κ_{electron} , and L are thermal conductivity due to lattice and electronic contributions and Lorentz number, respectively. We assume κ_{lattice} for the film is equal to measured value of the bulk single crystalline SrTiO_3 , which is independent of the Nb concentration ($3 \text{ Wm}^{-1}\text{K}^{-1}$). L was calculated using the observed S and n values for the films. As shown in Fig. 3(b), the electronic contribution to the thermal conduction does not become negligible when the carrier concentration exceeds 10^{21} cm^{-3} . The κ_{total} value increases with n when n exceeds $3 \times 10^{20} \text{ cm}^{-3}$ as clearly shown in the inset. Hence, we took the contribution of κ_{electron} into account to estimate the ZT values of the epitaxial films. The ZT values of the Nb-doped SrTiO_3 at 1000 K are plotted as a function of Nb content in Fig. 3(c). The ZT value increases with n , and it shows the maximum value of ~ 0.37 at $x=0.2$ ($n \sim 4.0 \times 10^{21} \text{ cm}^{-3}$) as a result of the reduction of ZT due to the enhancement of the thermal conductivity with the carrier concentration.

In summary, we clarified experimentally the maximum ZT value for Nb-doped SrTiO_3 at 1000 K in terms of carrier concentration. ZT of Nb-doped SrTiO_3 increases with the Nb concentration (x) and it reaches ~ 0.37 at $x=0.2$. Our results indicate that heavily Nb-doped SrTiO_3 is a good candidate for n -type thermoelectric oxide usable at high temperatures.

¹I. Terasaki, Y. Sasago, and K. Uchinokura, Phys. Rev. B **56**, 12685 (1997).

²R. Funahashi, I. Matsubara, H. Ikuta, T. Takeuchi, U. Mizutani, and S. Sodeoka, Jpn. J. Appl. Phys., Part 2 **39**, L1127 (2000).

³R. Funahashi and M. Shikano, Appl. Phys. Lett. **81**, 1459 (2002).

⁴M. Mikami, R. Funahashi, M. Yoshimura, Y. Mori, and T. Sasaki, J. Appl. Phys. **94**, 6579 (2003).

⁵Oxide Thermoelectrics, edited by K. Koumoto *et al.* (Research Signpost, 2002).

⁶B. A. Cook, J. L. Harringa, S. H. Hann, and C. B. Vining, J. Appl. Phys. **78**, 5474 (1995).

⁷I. Nishida, Phys. Rev. B **7**, 2710 (1973).

⁸M. Ohtaki, T. Tsubota, K. Eguchi, and H. Arai, J. Appl. Phys. **79**, 1816 (1996).

⁹H. Ohta, W.-S. Seo, and K. Koumoto, J. Am. Ceram. Soc. **79**, 2193 (1996).

¹⁰S. Isobe, T. Tani, Y. Masuda, W.-S. Seo, and K. Koumoto, Jpn. J. Appl. Phys., Part 1 **41**, 731 (2002).

¹¹H. P. R. Frederikse, W. R. Thurber, and W. R. Hosler, Phys. Rev. **134**, A442 (1964).

¹²T. Okuda, K. Nakanishi, S. Miyasaka, and Y. Tokura, Phys. Rev. B **63**, 113104 (2001).

¹³F. J. DiSalvo, Science **285**, 703 (1999).

¹⁴S. Ohta, T. Nomura, H. Ohta, and K. Koumoto, J. Appl. Phys. **97**, 1 (2005).

¹⁵R. D. Shannon, Acta Crystallogr., Sect. A: Cryst. Phys., Diff., Theor. Gen. Crystallogr. **32**, 751 (1976).

¹⁶H. Ledbetter, M. Lei, and S. Kim, Phase Transitions **23**, 61 (1990).

¹⁷C. B. Vining J. Appl. Phys. **69**, 331 (1991).